



# Manipulating polydispersity of lens $\beta$ -crystallins using divalent cations demonstrates evidence of calcium regulation

Michael R. Bergman<sup>a</sup>, and Leila F. Deravi<sup>a,1</sup>

Edited by Rachel W. Martin, University of California Irvine, Irvine, CA; received July 18, 2022; accepted October 13, 2022 by Editorial Board Member Shaul Mukamel

Crystallins comprise the protein-rich tissue of the eye lens. Of the three most common vertebrate subtypes,  $\beta$ -crystallins exhibit the widest degree of polydispersity due to their complex multimerization properties *in situ*. While polydispersity enables precise packing densities across the concentration gradient of the lens for vision, it is unclear why there is such a high degree of structural complexity within the  $\beta$ -crystallin subtype and what the role of this feature is in the lens. To investigate this, we first characterized  $\beta$ -crystallin polydispersity and then established a method to dynamically disrupt it in a process that is dependent on isoform composition and the presence of divalent cationic salts ( $\text{CaCl}_2$  or  $\text{MgCl}_2$ ). We used size-exclusion chromatography together with dynamic light scattering and mass spectrometry to show how high concentrations of divalent cations dissociate  $\beta$ -crystallin oligomers, reduce polydispersity, and shift the overall protein surface charge—properties that can be reversed when salts are removed. While the direct, physiological relevance of these divalent cations in the lens is still under investigation, our results support that specific isoforms of  $\beta$ -crystallin modulate polydispersity through multiple chemical equilibria and that this native state is disrupted by cation binding. This dynamic process may be essential to facilitating the molecular packing and optical function of the lens.

lens | polydispersity | assembly |  $\beta$ -crystallin | divalent cations

Located in the center of the eye, the vertebrate lens has two primary functions—optical transparency and light refraction. These functions are enabled through a unique cell life cycle that concentrates proteins in a concentric pattern throughout the tissue prior to organelle degradation (1–3). Because of this, there is little protein turnover in the lens, necessitating life-long stability of the proteins to maintain a paracrystalline network (4). At a molecular level, the cytosol of the vertebrate lens largely consists of three proteins:  $\alpha$ ,  $\beta$ , and  $\gamma$ -crystallin. The subtype  $\alpha$ -crystallin is made of two subunits,  $\alpha\text{A}$  and  $\alpha\text{B}$ , and has been characterized as a small heat-shock protein (sHsp) to function as a nonspecific chaperone in the lens. The  $\beta\gamma$ -crystallins are part of a structural superfamily with seven  $\beta$ -crystallins (six genes, with one isoform pair resulting from alternative splicing) and six  $\gamma$ -crystallin variants in the human lens. While  $\gamma$ -crystallin remains monomeric in the lens,  $\beta$ -crystallin assembles into three commonly denoted subpopulations:  $\beta_{\text{H}}$ ,  $\beta_{\text{L1}}$ , and  $\beta_{\text{L2}}$ . Like the other two crystallin subtypes,  $\beta$ -crystallins have prescribed optical (5–9) and protective (10–12) functions. However, it is unclear why multiple oligomers persist within the  $\beta$ -crystallin subtype and what their specific roles are in the lens.

One proposed function for  $\beta$ - and  $\gamma$ -crystallins is calcium buffering (13–17). Calcium homeostasis in the vertebrate lens is regulated primarily by the epithelial layer; signaling is facilitated by cellular gap junctions and connexin proteins (13, 18–20). Although present in the lens, 99% of intracellular calcium is in a bound state (13, 21, 22), where either an increase or decrease in free calcium will result in lens opacities and cataracts (23, 24). On the other hand, aging and cataract progression change calcium distribution, its basal levels, and signaling across the lens (19, 21, 25, 26). This also leads to an increase in proteolytic activity from calpains I and II, which is linked to further protein aggregation (27, 28). Therefore, calcium buffering is vital to maintenance of lens transparency and cataract prevention. Other cations like magnesium and copper have also been implicated in tissue transparency, suggesting a broader role for cations (29). While the exact mechanism for calcium buffering remains unknown, it is clear that cation regulation is important for healthy lens function.

Another aspect of lens transparency is the short-range interactions between the crystallins (7, 30, 31), where protein polydispersity enables dense yet fluid packing without crystallization. For instance, in the squid lens, polydispersity is observed within the loop regions of a single S-crystallin subtype to achieve this function (32). Earlier work by Schurtenberger and Augusteyn confirmed that vertebrate  $\alpha$ -crystallins also exhibited polydispersity, which is expected to serve a similar purpose. In the vertebrate lens, there is also an extra dimension

## Significance

One common feature conserved across living systems is the presence of a high concentration of crystallin proteins packed within the eye lens. The polydispersity of crystallins in the vertebrate lens is one factor that may prevent crystallization from the dense protein array within lens fiber cells. We probe the spatial distribution and assembly mechanics of the  $\beta$ -subtype in bovine lens. We assay hydrodynamic behavior in different salts and observe altered protein polydispersity *in vitro*. Our results describe reversible changes in size and surface charge of  $\beta$ -oligomers that are regulated by divalent cations. Our data suggest a dynamic equilibrium that produces the inherent polydispersity of  $\beta$ -crystallin as an important feature of lens function and stability.

Author affiliations: <sup>a</sup>Department of Chemistry and Chemical Biology, Northeastern University, Boston, MA 02115

Author contributions: M.R.B. and L.F.D. designed research; M.R.B. performed research; M.R.B. analyzed data; and M.R.B. and L.F.D. wrote the paper.

The authors declare no competing interest.

This article is a PNAS Direct Submission. R.W.M. is a guest editor invited by the Editorial Board.

Copyright © 2022 the Author(s). Published by PNAS. This open access article is distributed under [Creative Commons Attribution-NonCommercial-NoDerivatives License 4.0 \(CC BY-NC-ND\)](https://creativecommons.org/licenses/by-nc-nd/4.0/).

<sup>1</sup>To whom correspondence may be addressed. Email: l.deravi@northeastern.edu.

This article contains supporting information online at <https://www.pnas.org/lookup/suppl/doi:10.1073/pnas.2212051119/-/DCSupplemental>.

Published November 22, 2022.

of polydispersity afforded by  $\beta$ -crystallins, present as dimers through octamers, which has further been linked to maintaining osmotic pressure gradients needed for proper refraction in the lens (6, 8, 9). Despite these important connections, it is still unknown how multiple isoforms of this one subtype combine and coordinate with such a high degree of fidelity to establish the necessary polydispersity required for packing in the lens. Studies using lens-purified or recombinantly expressed  $\beta$ -crystallin isoforms revealed acid–base interactions at the N- and C-termini associated with homo- and heterodimerization (33–42). Other reports highlighted solvent accessibility (43), sequence length (40, 44, 45), and terminus composition (46, 47) of select isoforms as relevant variables that impact pairings and downstream protein assembly. The exception is  $\beta$ B2 which does not have these extensions (48–50). Additionally, interactions including hydrogen-bonding or hydrophobic contacts (50–53) have also been highlighted in  $\beta$ -crystallin assembly, where destabilizing post-translational modifications at the dimer interface may disrupt the integrity of the broader lens structure (54, 55).

Based on these past reports, it is clear that there is a vital role for noncovalent interactions in  $\beta$ -crystallin oligomerization, where these transient bonds are driven by entropy to support proper lens function (35, 41, 56, 57). We developed conditions that impact these interactions and, as a result, the polydispersity of bovine lens  $\beta$ -oligomers in vitro. Given the susceptibility for salt bridges across the  $\beta$ -crystallin isoforms, we chose to first explore the role of ions and ionic strength on regulating assembly dynamics. Similar to Morais et al. who studied the effects of divalent cations on the dimer–decamer equilibrium of 2-Cys peroxidoreductins (58), we utilized size-exclusion chromatography (SEC) and dynamic light scattering in the presence of cationic salts ( $\text{MgCl}_2$  and  $\text{CaCl}_2$ ) to investigate how oligomer size and surface charge adapted as we forced the distribution from larger multimers to trimers and dimers with increasing salt concentrations. We then explored the reversibility of this salt-based assay to probe potential pathways for oligomerization. When taken together, our results add a fresh perspective on  $\beta$ -crystallin assembly dynamics, highlighting key properties that enable or disrupt their polydispersity in the lens.

## Results

**$\beta$ -crystallin Polydispersity Across the Lens.** We began our analysis of protein polydispersity by first interrogating the relative proportions of  $\beta_{\text{H}}$ ,  $\beta_{\text{L1}}$ , and  $\beta_{\text{L2}}$  across a bovine lens. To start, each lens was dissected concentrically to create segments labeled as the nucleus, inner cortex, and outer cortex (Fig. 1A). Each segment was then homogenized and purified separately with SEC and eluted with phosphate-buffered saline (PBS), pH 7.3, producing up to six crystallin populations. Sodium dodecyl sulfate–polyacrylamide-gel electrophoresis (SDS–PAGE) analysis was used on whole-lens lysate to match crystallin identities with their respective elution volumes (*SI Appendix, Fig. S1*). Additionally, we used liquid chromatography tandem mass-spectrometry (LC–MS/MS) on eluted fractions to confirm the presence of  $\alpha$ -crystallin (sometimes referred to as high- and low-molecular weight  $\alpha$ -crystallin:  $\alpha$  and  $\alpha_{\text{L}}$ , respectively),  $\beta_{\text{H}}$ ,  $\beta_{\text{L1}}$ ,  $\beta_{\text{L2}}$ , and  $\gamma$ -crystallin, which were comparable with previously published results (33, 35, 37, 59, 60). Based on a protein standard curve, we estimated molecular weights of eluents from SEC as 212 kDa ( $\beta_{\text{H}}$ ), 72 kDa ( $\beta_{\text{L1}}$ ), and 43 kDa ( $\beta_{\text{L2}}$ ), which also compared favorably with previous reports (34, 44). Even though our  $\beta_{\text{H}}$  fraction had a higher predicted molecular weight than expected, the calculated  $\beta_{\text{L1}}$  and  $\beta_{\text{L2}}$  sizes supported the presence of trimers and dimers, respectively.

The chromatographic results from the purification of nuclear and cortical lens segments indicated clear changes in all crystallin subtypes across the lens (Fig. 1B). Because the mass of each crystallin subtype was collected and compared with the standardized loaded mass, all results were linked to direct changes in polydispersity based on location (Fig. 1C). Using this approach, we observed that the concentration of  $\alpha$ - and  $\gamma$ -crystallins was the highest in the nucleus and decreased toward the outer cortex and that all  $\beta$ -crystallin oligomers appeared to be more concentrated in the lens cortex, which again were all consistent with previous reports (61–63). When combined, the  $\beta$ -crystallins accounted for 24.4% of total protein in the outer cortex, making them the most abundant subtype in this location. Comparing the nucleus and outer cortex, we observed  $\beta_{\text{H}}$  and  $\beta_{\text{L2}}$  abundance that was approximately 2 $\times$  higher in the outer cortex, while  $\beta_{\text{L1}}$  was approximately 7 $\times$  higher. From each segment of the lens,  $\beta_{\text{H}}$  was the most abundant form; however, the relative distribution of the oligomers varied across the lens. In the nucleus,  $\beta_{\text{H}}$ ,  $\beta_{\text{L1}}$ , and  $\beta_{\text{L2}}$  were present at an approximately 14:1:6 mass ratio, which decreased to a 4.5:1:2.2 mass ratio at the outer cortex. Because the injected mass was standardized, these differences indicated a persistent distribution and suggested that  $\beta$ -crystallin polydispersity was not solely dependent on concentration. Instead, it is possible that variations within native isoform abundance produced these differences.

We next investigated compositional differences between  $\beta$ -subpopulations. Previous reports have indicated that not all  $\beta$ -crystallin isoforms are present across  $\beta_{\text{H}}$ ,  $\beta_{\text{L1}}$ , and  $\beta_{\text{L2}}$  (33, 36, 37, 53). However, our mass spectrometry analysis of the  $\beta_{\text{H}}$  and  $\beta_{\text{L2}}$  fractions from a whole-lens lysate indicated similar sample compositions and identified peptides corresponding to every  $\beta$ -crystallin isoform in both (Fig. 1D). A comparison of the normalized peptide counts showed differences between  $\beta_{\text{H}}$  and  $\beta_{\text{L2}}$ , where  $\beta\text{A1/A3}$ ,  $\beta\text{A4}$ , and  $\beta\text{B1}$  isoforms were more abundant in the  $\beta_{\text{H}}$  fractions. These results are in good agreement with previous reports (64, 65). Using the ratios for each isoform from the normalized peptide spectral matches (PSM), we generated a scale that indicated the probability for each isoform being present in the  $\beta_{\text{H}}$  or  $\beta_{\text{L2}}$  fractions (Fig. 1D, *Inset*). No trend or grouping was observed for either acidic or basic isoforms in our analysis. Rather,  $\beta\text{B1}$  was most likely to be found at higher proportions in larger  $\beta$ -oligomers ( $\beta_{\text{H}}$ ) at a  $\sim$ 5:1 ratio, and  $\beta\text{B2}$  was more likely to be found at higher proportions in smaller  $\beta$ -oligomers ( $\beta_{\text{L2}}$ ) at a  $\sim$ 1:2 ratio. These data indicated that all isoforms were capable, and possibly required, to produce polydispersity.

**Effects of Divalent Cations on  $\beta$ -crystallin Polydispersity.** While there are several known interactions that promote oligomerization of  $\beta$ -crystallins, we chose to first explore the role of ions and ionic strength on regulating assembly dynamics. It is known that  $\beta$ -crystallins retain a weak-to-moderate affinity for binding  $\text{Ca}^{2+}$  (14, 66, 67), and early characterizations showed trace amounts of magnesium and calcium present in both  $\beta_{\text{H}}$  and  $\beta$ -L (combined  $\beta_{\text{L1}}$  and  $\beta_{\text{L2}}$ ) fractions (34). We evaluated how increasing concentrations of  $\text{MgCl}_2$  (Fig. 2) or  $\text{CaCl}_2$  (*SI Appendix, Fig. S2*) changed oligomer distribution. At concentrations of 0.01 and 0.1 M  $\text{MgCl}_2$ , there was a negligible effect on the elution profile of lens crystallins compared with physiological salt levels (Fig. 2A and *SI Appendix, Fig. S3*). Specifically, there were minimal changes in peak area, where the notable differences were an approximately 3% decrease in  $\beta_{\text{H}}$  and corresponding increase in  $\beta_{\text{L2}}$  between the conditions. When salt concentration increased to 1 M, we observed an unexpected dissociation of  $\beta_{\text{H}}$  oligomers in the eluate with an

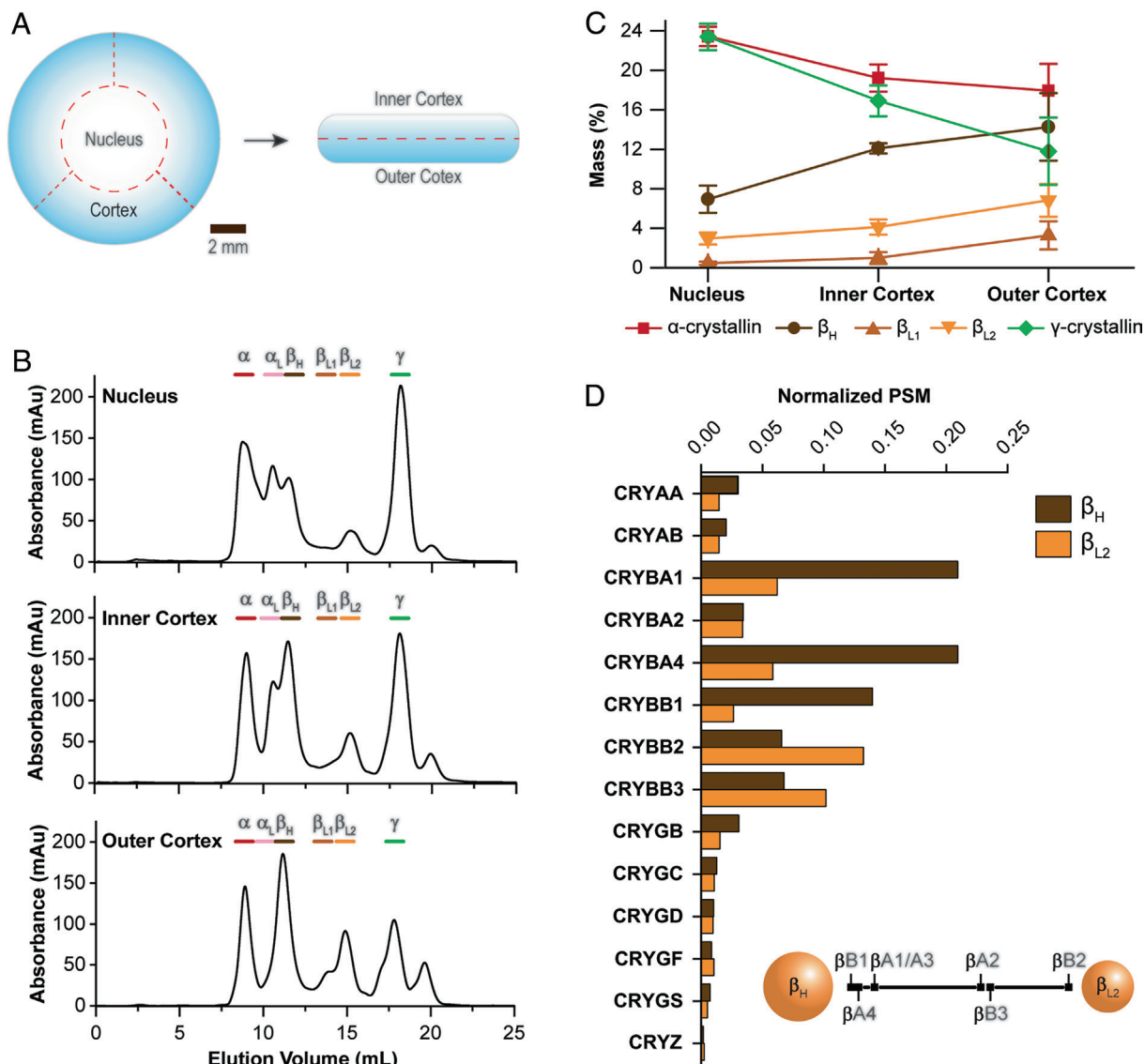


**Fig. 1.** Correlations between tissue location, isoform composition, and  $\beta$ -crystallin quaternary structure. (A) Diagram of how each lens segment was prepared. Lens segments were lysed separately and purified in PBS, pH 7.3. (B) Representative chromatograms obtained from the nuclear, inner cortical, and outer cortical segments of the lens. In each case, 3 mg of protein was loaded. Elution volumes corresponding to each crystallin population are denoted on *Top*. (C) Comparison of changes in crystallins based on mass (%) across the lens showed a gradient of  $\beta$ -crystallins that was most concentrated in the lens cortex. Data points were averaged from biological replicates ( $N = 3$ ) with error bars representing one SD. (D) Peptides corresponding to bovine crystallins were positively detected ( $\geq 95\%$  confidence) and confirmed the presence of 15 crystallins in both  $\beta_H$  and  $\beta_{L2}$ . Above is a scale of the ratios of normalized PSM matching  $\beta$ -crystallin isoforms detected in both  $\beta_H$  and  $\beta_{L2}$ . From this,  $\beta B1$  was most prevalent in larger oligomers ( $\beta_H$ ) while  $\beta B2$  was most prevalent in smaller  $\beta$ -oligomers ( $\beta_{L2}$ ).

average decrease of 25.6% in the total area between 0.01 M and 1 M  $MgCl_2$ . This decrease corresponded to an average increase of 23.3% observed in the  $\beta_{L2}$  population (Fig. 2B), suggesting a direct conversion between the two. There also appeared to be an increase in  $\beta_{L1}$  formation along with a decrease in  $\alpha$ -crystallin eluted with 1 M  $MgCl_2$ . The decrease in  $\alpha$ -crystallin may be due to a decreased solubility under higher ionic conditions and formation of larger aggregates that do not enter the size-exclusion matrix. For the nonnormalized data (SI Appendix, Fig. S4), we observed an increase in the total area-under-the-curve that correlated consistently with increased  $Mg^{2+}$  concentration. This was unexpected, since  $Mg^{2+}$  alone does not absorb at 280 nm. Recently, it has been shown that amino acid coordination of divalent cations can increase ultraviolet (UV) absorption and has been observed with even Gly- $Mg^{2+}$  complexes in vitro (68), suggesting metal coordination can impact optical signatures of amino acids alone. While we suspect similar interactions are involved in our samples, we expect that

the chromatographic profiles are affected proportionally. For this reason, we report calculated area as a percentage to account for these changes (Fig. 2B).

We used LC-MS/MS to compare collected fractions corresponding to  $\beta_{L2}$  purified under 1 M salt to those eluted with PBS (SI Appendix, Fig. S5). From the results, we confirmed 79 of the 134 originally identified proteins; unique peptides matching all  $\beta$ -crystallin isoforms were again detected in both. We found that the 1 M salt purified  $\beta_{L2}$  fractions contained increased amounts of  $\beta A1/3$ ,  $\beta A4$ , and  $\beta B1$  – all of which were involved with formation of  $\beta_H$  oligomers. Although  $\beta_H$  has been shown to partially dissociate with pH or higher ionic strength, this is a condition where near complete dissociation of  $\beta_H$  to trimers ( $\beta_{L1}$ ) and dimers ( $\beta_{L2}$ ) was achieved in vitro.

We next investigated whether these relationships were specific to divalent cations. We assessed the effects of ionic strength by comparing purifications in 0.33 M  $MgCl_2$  and 1 M NaCl. In 1

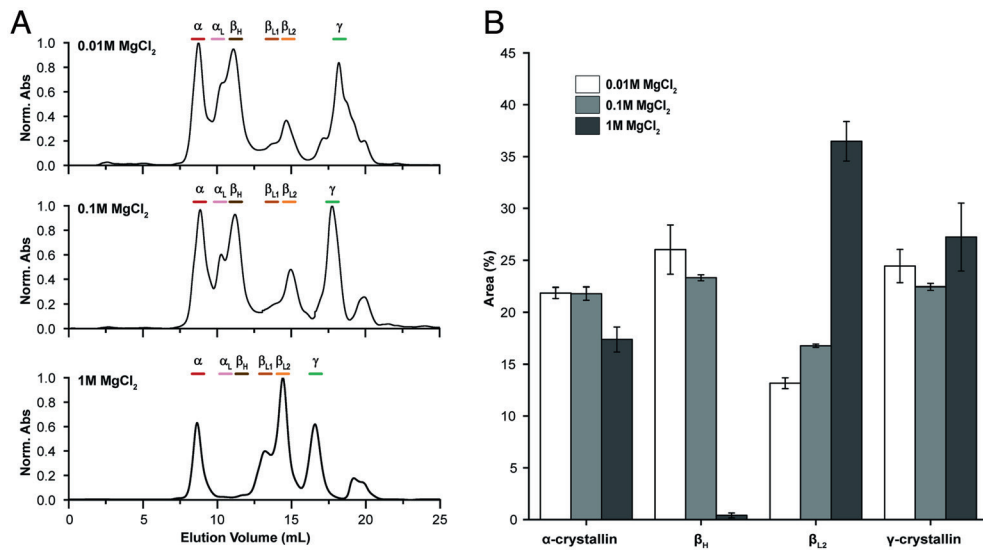


**Fig. 2.** MgCl<sub>2</sub> alters oligomer distribution of  $\beta$ -crystallins. (A) Purifications of whole lens lysates eluted with 10 mM Tris, pH 7.3, with either 0.01, 0.1, or 1 M MgCl<sub>2</sub>. Three milligrams of protein were loaded for each condition; absorbance has been normalized for more clear comparison. Retention times are similar for  $\alpha$ - and  $\beta$ -crystallins across the three conditions. (B) Significant changes in  $\beta_{\text{H}}$  and  $\beta_{\text{L}2}$ , as well as a change in  $\alpha$ -crystallin, were observed as the larger oligomers dissociated in increasing levels of divalent cations. Data were averaged for biological replicates ( $N = 3$ ) with error bars representing one SD.

M NaCl there were negligible changes compared with physiological salt levels (maximum difference of 4% area across all crystallins, *SI Appendix, Fig. S6*). Because we consistently observed that divalent cation solutions (1 M total ionic strength) were needed to dissociate  $\beta_{\text{H}}$ , we next pushed this idea further by purifying in even higher ionic strength conditions (1.5 M NaCl) and again noted minimal changes in the amount of  $\beta_{\text{H}}$  with an average additional difference of 2% between 1 and 1.5 M NaCl (*SI Appendix, Fig. S6C*). Despite the minimal change in  $\beta_{\text{H}}$ , we did observe an 8.2% increase in  $\beta_{\text{L}2}$  and 6.5% increase in  $\gamma$ -crystallin under 1.5 M NaCl, as well as a total loss in the  $\alpha_{\text{L}}$  peak, indicating a threshold ionic strength value that may impact other subtypes but not  $\beta$ -crystallins. When taken together, our data revealed specific interactions unique to divalent cations with  $\beta$ -crystallins that extend beyond simple charge-based screening to disrupt polydispersity.

**Adsorption of Divalent Cations as a Mechanism for  $\beta_{\text{H}}$  Oligomer Dissociation.** Given the highly specific structural changes observed in the presence of MgCl<sub>2</sub> and CaCl<sub>2</sub>, we investigated the electrical double-layer of our proteins in solution via zeta-

potential measurements across a wide pH range (pH 3–8). Because zeta-potential is a measurement of the electrochemical surface of colloidal particles (e.g., protein oligomers), we could directly probe whether Mg<sup>2+</sup> was adsorbed to the surface through isoelectric point (pI) calculations of crystallin mixtures. The advantage of this method was its ability to characterize heterogeneous mixtures, such as the lens crystallins, while in solution.

To begin, we collected  $\alpha$ ,  $\beta_{\text{H}}$ , and  $\beta_{\text{L}2}$  crystallins in PBS and analyzed them in a custom phosphate-citrate-carbonate saline (PCCS) buffer, which allowed us to better control changes in pH over the course of the experiment. We compared these data with measurements in buffers containing 0.01 or 0.1 M MgCl<sub>2</sub>, selected to retain the original  $\beta_{\text{H}}$  population. Here, pI is defined by regions where the zeta-potential is 0 mV (gray dashed line, Fig. 3). The control conditions (Fig. 3, black squares) indicated that  $\alpha$ ,  $\beta_{\text{H}}$ , and  $\beta_{\text{L}2}$  crystallins have anionic surface charges at physiological pH with pI of 4.53, 5.21, 4.97, respectively (Table 1). It was interesting that  $\beta_{\text{H}}$  and  $\beta_{\text{L}2}$ , both heterogeneous mixtures composed of similar isoforms, exhibited different surface charges. In the presence of 0.01 or 0.1 M MgCl<sub>2</sub>, the first noted change was that the magnitude of zeta-potential at all pH decreased. This was an

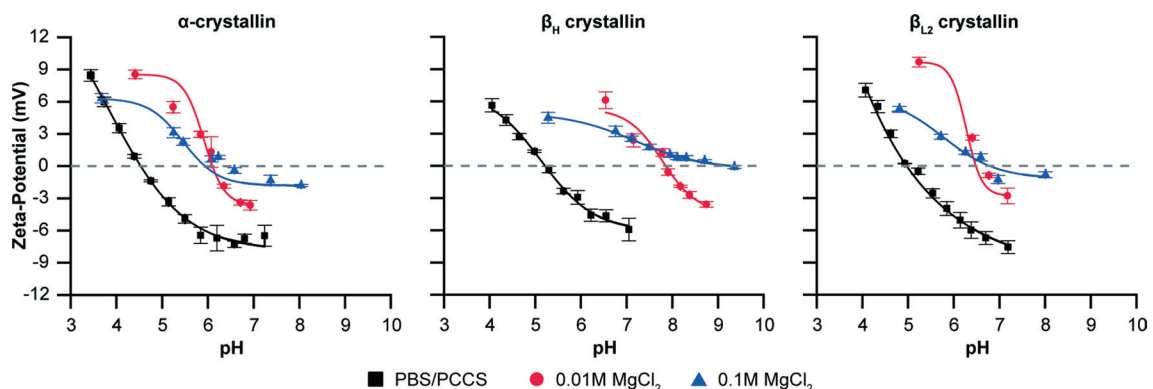


**Fig. 3.** Oligomer dissociation through adsorption of divalent cations. Isoelectric points were determined by measurement of the zeta-potential as the sample was titrated with 0.1 M HCl. Crystallins were either purified in PBS or 10 mM Tris, pH 7.3 with 0.01 or 0.1 M MgCl<sub>2</sub>. PBS-purified samples were diluted with phosphate-citrate-carbonate saline buffer. Each data point was averaged from five measurements with error bars representing one SD (one biological replicate,  $N = 1$ ). All lines were fitted using a sigmoidal function (adjusted  $R^2$  values between 0.9052 and 0.9964).

**Table 1. Calculated isoelectric points of  $\alpha$  and  $\beta$ -crystallins in the presence of  $Mg^{2+}$** 

	PBS	0.01 M $MgCl_2$	0.1 M $MgCl_2$
$\alpha$ -crystallin	4.53	6.13	6.53
$\beta_H$	5.21	7.85	9.28
$\beta_{L2}$	4.97	6.48	6.78

anticipated effect due to compression of the electrical double-layer under increased ionic strength (69). The apparent pI under each condition increased by +1.60, +2.64, and +1.51 in 0.01 M  $MgCl_2$  and +2.00, +4.07, and +1.81 0.1 M  $MgCl_2$  for the  $\alpha$ ,  $\beta_H$ , and  $\beta_{L2}$  fractions, respectively (Table 1). While increasing  $Mg^{2+}$  concentrations also increased the pI of the other subtypes measured, the dramatic changes specific to  $\beta_H$  suggested a unique interaction between  $\beta_H$  oligomers and  $Mg^{2+}$ . This may be due to the exposed surface area and chemistry specific to the  $\beta_H$  oligomers.

After establishing the connection between ionic valency and  $\beta$ -crystallin polydispersity, we next asked if the proteins were equally sensitive to the presence of divalent anions. We used 0.33 M  $Na_2SO_4$  and observed no significant changes in elution profiles compared with the control, with pI decreases of -0.9, -0.93, and -1.1 for  $\alpha$ ,  $\beta_H$ , and  $\beta_{L2}$ , respectively (SI Appendix, Fig. S7 and Table S1). Although the slight negative shift observed here supported anion adsorption (at 3 $\times$  the  $MgCl_2$  concentration used above), the altered surface charge did not impact oligomerization. This further supported that there was potential competition between divalent cations and stability of  $\beta_H$  oligomers.

**Dissociation and Reassociation of  $\beta$ -crystallins with  $Mg^{2+}$ .** We next used our cation-SEC assay to interrogate the oligomerization of  $\beta$ -crystallins. We chose to use  $MgCl_2$  instead of  $CaCl_2$  to mitigate calcium-induced crystallin aggregates (70, 71) and avoid precipitation with phosphate buffers. To start, we purified whole lens lysate in PBS to collect the  $\beta_H$  fractions. We next dissociated  $\beta_H$  in 10 mM Tris containing 1 M  $MgCl_2$ , generating both  $\beta_{L1}$  (35.4%) and  $\beta_{L2}$  (52.8%), with some  $\alpha$ -crystallin present as well (8.9%, Fig. 4A). Separately, we isolated  $\beta_{L1}$  and  $\beta_{L2}$  fractions in 1 M  $MgCl_2$  from whole lens lysate, then assayed its potential for reassociation when reloaded into PBS containing ethylenediaminetetraacetic acid (EDTA). For the  $\beta_{L2}$  fraction, we observed a reassociation into  $\beta_H$  oligomers with some formation of  $\beta_{L1}$  accounting for 12.4% of the total area (Fig. 4B). For the  $\beta_{L1}$  fraction, we observed a greater  $\beta_H$  reassociation of 62.5% (Fig. 4B) compared with 27.6% with  $\beta_{L2}$ , with minimal dissociation of  $\beta_{L1}$  to  $\beta_{L2}$  (Fig. 4C). Without the addition of EDTA, no  $\beta_{L1}$  formation was observed, and there was less  $\beta_H$  formed as well, suggesting that residual  $Mg^{2+}$  may have continued to inhibit formation of  $\beta_{L1}$  and  $\beta_H$  (SI Appendix, Fig. S8).

As a final variable, we asked whether the presence of  $\alpha$ -crystallin, a native chaperone in the lens, could impact reassociation of  $\beta_H$ . To test this, isolated  $\alpha$ -crystallin purified in PBS was mixed in a 1:1 mass ratio with the  $\beta_{L2}$  fraction in 1 M  $MgCl_2$  and reloaded with PBS (Fig. 4D). We chose not to include EDTA in the reloaded buffer for this experiment to better assess whether  $\alpha$ -crystallin had a comparable effect to EDTA in removing ions. The result was similar to reassociation of  $\beta_{L2}^{(Mg)}$  but with no distinct formation of  $\beta_{L1}$ , suggesting that  $\alpha$ -crystallin was less effective than EDTA in reassociating  $\beta$ -crystallins from  $Mg^{2+}$  conditions (Fig. 4E). In both cases, the removal of  $Mg^{2+}$  resulted in the reassociation of larger oligomers ( $\beta_H$ ) in a process that was independent of  $\alpha$ -crystallin. Moreover, simple reinjection alone did not

reassociate the oligomers (SI Appendix, Fig. S9), further supporting the need for specific isoforms in eliciting these effects.

While we reproducibly observed dissociation of  $\beta_H$  oligomers in the presence of high (1 M) divalent cationic salts, our assay did not yield  $\beta$ -substructures smaller than dimers. Because monomeric  $\beta$ -crystallin was not observed from lens lysates nor cationic dissociation, we concluded, as others have previously (38, 42), that the equilibrium of  $\beta$ -crystallin greatly favors higher order structures. From these observations and our own data, we propose a pathway for  $\beta$ -crystallin multimerization and polydispersity (Fig. 5). Since  $\beta_{L2}$  is always observed in greater amounts than  $\beta_{L1}$  in the lens, we might expect that  $K_1 > K_2$ , but this is not necessarily true and they may be similar. The greater amounts of  $\beta_{L2}$  could also be explained by  $K_3 > K_4$ , which is supported by the increased reassociation from  $\beta_{L1}$  to  $\beta_H$  compared with  $\beta_{L2}$  (Fig. 4). Lastly, because we observed some interconversion between  $\beta_{L1}$  and  $\beta_{L2}$  when using EDTA, a minor equilibrium between the two may also exist, denoted as  $K_5$  (Fig. 5). Overall, when combined with our SEC and mass spectrometry data, this model suggests two competing interactions may be involved in lens  $\beta$ -crystallin oligomerization: protein-protein and protein-cation interactions.

**Probing Hydrophobic Interfaces.** Previous studies have outlined the presence of hydrophobic interactions in the assembly of  $\beta$ -crystallins (50–52), where histidine residues are important in the quaternary structure of larger  $\beta_H$  oligomers (53). Since it is known that hydrophobic interfaces play a role in  $\beta$ -crystallin assembly (50–52), we used SYPRO Orange as a fluorescent probe to approximate relative differences in hydrophobic surface area between  $\beta_H$  and  $\beta_{L2}$  at fixed concentrations (0.5 mg/mL) across the different solvent conditions (Fig. 6). Our results show that  $\beta_H$  oligomers have more solvent exposed hydrophobic surface area compared directly with  $\beta_{L2}$  at the 10 mM Tris condition based on its ~40% increased fluorescence (Fig. 6A). We observed a similar result in PBS (SI Appendix, Fig. S10), suggesting that no additional hydrophobic interfaces are involved in the assembly of native oligomers larger than tetramers. At 0.1 M  $MgCl_2$ , this difference is less pronounced (~23%, Fig. 6B). When cations are bound, we observed a ~47% decrease in fluorescence of  $\beta_H$  and a ~40% decrease in  $\beta_{L2}$  at 0.1 M  $MgCl_2$  compared with the original 10 mM Tris condition (Fig. 6B). Because the presence of  $MgCl_2$  decreases overall fluorescence in both  $\beta_H$  and  $\beta_{L2}$ , we believe that surface adsorption of  $Mg^{2+}$  may be near hydrophobic residues of the proteins to disrupt SYPRO Orange binding. We observed minimal changes in fluorescence between 0.1 M and 1 M  $MgCl_2$  (Fig. 6C), indicating that once  $Mg^{2+}$  is bound, there are no further changes in  $\beta_{L2}$  structure. These observations are consistent between replicates (Fig. 6D). Separately, our data reveal that hydrophobic interactions may play a stronger role in forming the  $\beta$ -L structures, but larger structures (i.e.,  $\beta_H$ ) appear to incorporate alternative mechanisms of assembly. While we cannot confirm the exact mechanism of these interactions, our results support that the binding of divalent cations disrupts some quaternary interfaces; this is further validated in our assay, as  $\beta$ -L structures remain intact when  $\beta_H$  consistently dissociated at higher (1 M)  $MgCl_2$ .

## Discussion

Our cation-based assay revealed three features associated with lens  $\beta$ -crystallins: 1) divalent cations dissociate large oligomers, 2) isoform abundance is a key component of oligomerization, and 3) a chemical equilibrium intrinsic to  $\beta$ -crystallins promotes its polydispersity. Specifically, our data support that oligomer dissociation

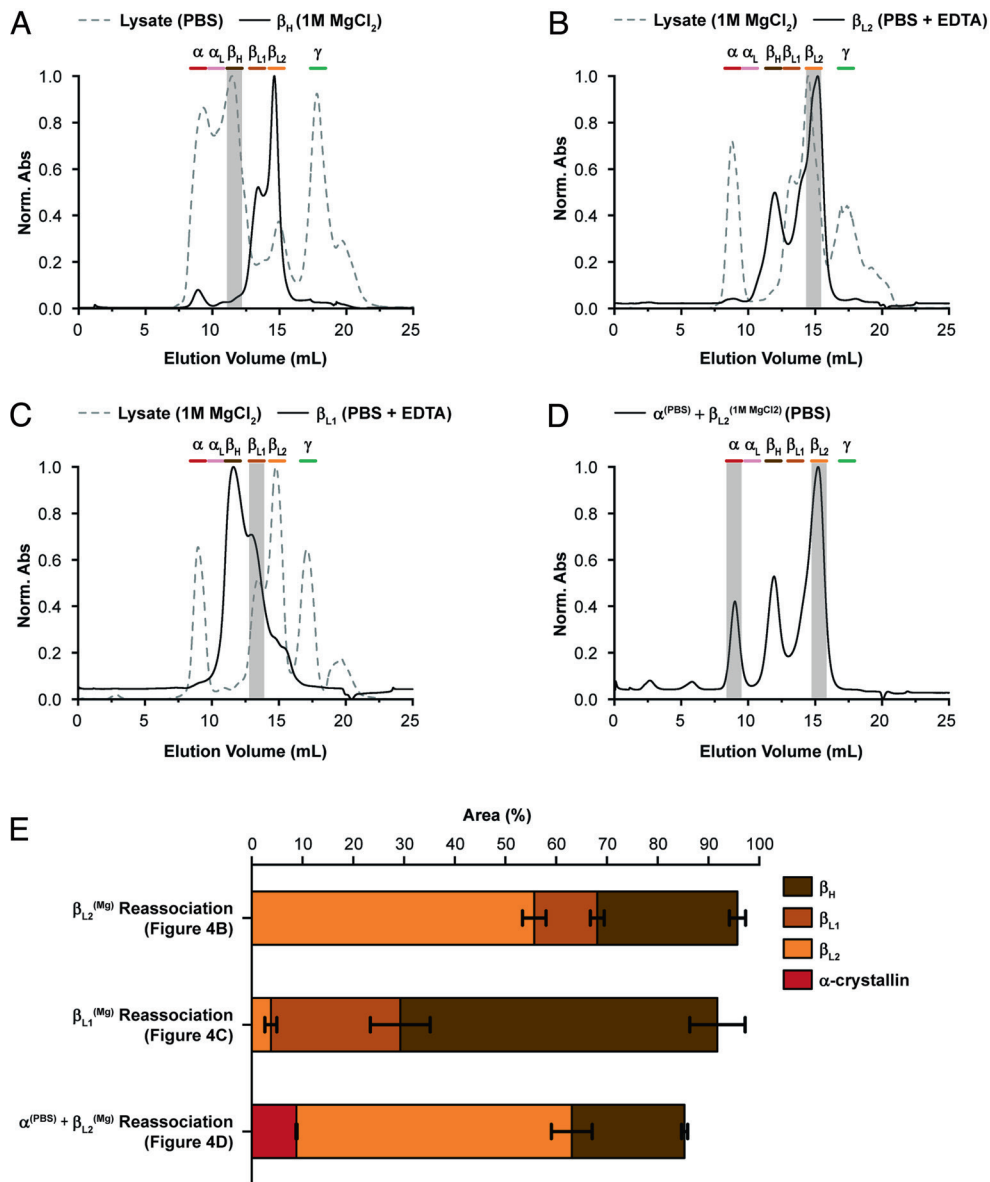


**Fig. 4.** Reassociation of  $\beta$ -oligomers shows assembly pathway from  $\beta_{L1}$  or  $\beta_{L2}$  to  $\beta_H$ . In *A–D*, gray dashed lines represent the initial purification to recover select fractions. Solid black lines represent the experimental condition during reelution of selected subtypes or mixtures. (*A*) Whole-lens lysate was purified in PBS (gray dashed line), and the  $\beta_H$  fractions (gray highlighted) were collected. Then,  $\beta_H$  was reeluted with buffer containing 1 M  $MgCl_2$  to dissociate  $\beta_H$  (solid black line). (*B*) Whole-lens lysate was purified in buffer containing 1 M  $MgCl_2$  (gray dashed line) and both the  $\beta_{L1}$  and  $\beta_{L2}$  fractions (gray highlighted) were collected, following reelution with PBS + 5 mM EDTA (solid black line). (*C*) Same as *B*, except  $\beta_{L1}$  (gray highlighted) was collected in 1 M  $MgCl_2$  and reeluted into PBS (solid black line). (*D*)  $\alpha$ -crystallin, purified in PBS, and  $\beta_{L2}$ , purified in 1 M  $MgCl_2$ , were mixed in a 1:1 mass ratio (total of 0.25 mg), and reeluted in PBS, pH 7.3. (*E*) AUC values for each of the previous chromatograms in *B–D*. Values are averages of biological replicates ( $N = 3$ ) with error bars representing one SD.

is a specific effect of divalent cation binding, indicating an additional interaction that should be considered along with charge-based interactions or salt bridges to describe crystallin assembly in the lens. We discuss interactions that may be conserved within the Greek-key motif involving acidic and polar residues to enable or disrupt  $\beta_H$  oligomerization transiently. Because all isoforms are present in all  $\beta$ -structures, oligomerization cannot be regulated by only one. We expect that a multistep chemical equilibrium promotes higher order assembly, where certain isoforms (A1/3, A4, and B1) appear as limiting reagents to complete oligomerization. Without these additional isoforms, there is negligible reassociation of smaller  $\beta$ -crystallin substructures to  $\beta_H$  (*SI Appendix, Fig. S9*).

The clear relationship between protein quaternary structure and the presence of divalent cations appears specific to  $\beta$ -crystallins, where near complete dissociation of  $\beta_H$  to  $\beta_{L1}$  (trimers) and  $\beta_{L2}$  (dimers) is achieved in vitro. This observation is unique and

introduces questions as to why there is such a high degree of structural complexity within the vertebrate  $\beta$ -crystallin subtype and what the role of this feature is in the vertebrate lens, as it is not often observed in other systems. For instance, structurally homologous  $\beta\gamma$ -crystallins in other organisms typically exist as monomers outside the lens, which bind cations in this monomeric state (67, 72–76). Vertebrate lens  $\beta$ -crystallins also retain binding affinity for calcium and other divalent cations. In fact, recombinantly expressed  $\beta$ -crystallin isoforms ( $\beta B2$  and  $\beta A3$ ) present a large range of dissociation constants ( $K_D$ ) between 40  $\mu M$  and 2.7 mM (14), suggesting significant variability between isoforms. In addition, even earlier reports of  $\beta_H$  crystallin harvested from rat lenses describe  $K_D$ 's ranging from 0.8  $\mu M$  to 300 mM (66, 70). Interestingly, the amount of detected calcium and magnesium has also been observed in higher abundance within  $\beta_H$  compared with  $\beta$ -L fractions in past reports (34). In our

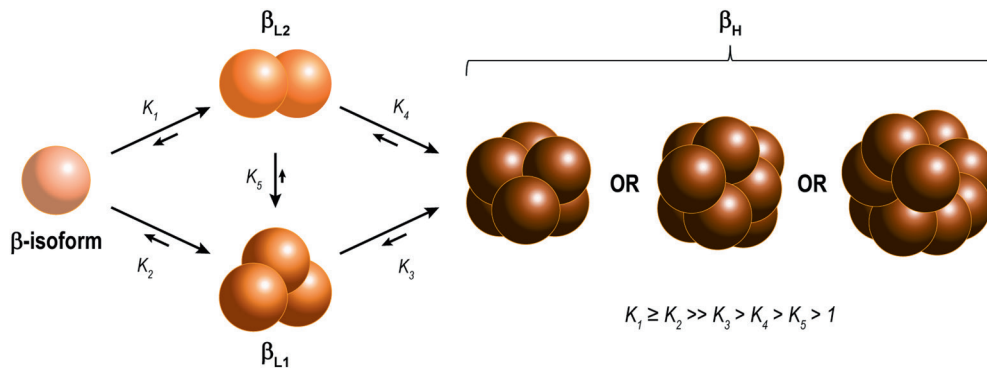


**Fig. 5.** The proposed multistep chemical equilibrium for higher order assembly of  $\beta$ -crystallin based on experimental evidence from dissociation and selective reassociation. Individual isoforms associate as dimers ( $\beta_{L2}$ ) or trimers ( $\beta_{L1}$ ), with possible low levels of interconversion between the two ( $K_5$ ). Equilibrium will preferentially drive assembly further into  $\beta_H$  oligomers, forming hexamers, octamers, and potentially nonamers. All reactions are expected to be product favored. This schematic does not highlight the possibility of a newly synthesized isoform and an existing dimer ( $\beta_{L2}$ ) to combine and form a trimer ( $\beta_{L1}$ ). This combination is not supported nor refuted by our experimental data. We would expect that path to be a competing equilibrium with  $K_2$ .

experiments, we intentionally saturated the microenvironment of our lens lysate with free  $\text{Ca}^{2+}$  to overcome the weaker binding affinities of  $\beta$ -crystallins to better observe potential effects in vitro. Our data further support increased cation coordination in larger oligomers (Table 1). In our studies, we observe initial oligomer dissociation with divalent cations at 100 mM and almost complete loss at 1 M—a range that exceeds the previously reported  $K_D$  values and more importantly infers some mechanistic insight, where interactions with divalent cations compete directly for sites of protein–protein interactions that ultimately force disassociation of  $\beta_H$  structures.

We are not the only ones to observe specific divalent cation-binding interactions within the  $\beta$ -subtype. In a study using a  $\beta$ -crystallin homolog, protein S sequenced from *Myxococcus xanthus*, Scholl et al. found that the presence of calcium stabilizes a single conformation of the N-terminal domain (77). Without calcium, the N-terminal domain can adopt two alternative conformations. Presumably, the lens  $\beta$ -crystallins could be affected similarly to protein S in the presence of elevated levels of  $\text{Ca}^{2+}$  or  $\text{Mg}^{2+}$ , where the N terminus involved in oligomerization is affected. We extend this hypothesis and propose a possible mechanism by which the cation-stabilized conformation is more thermodynamically

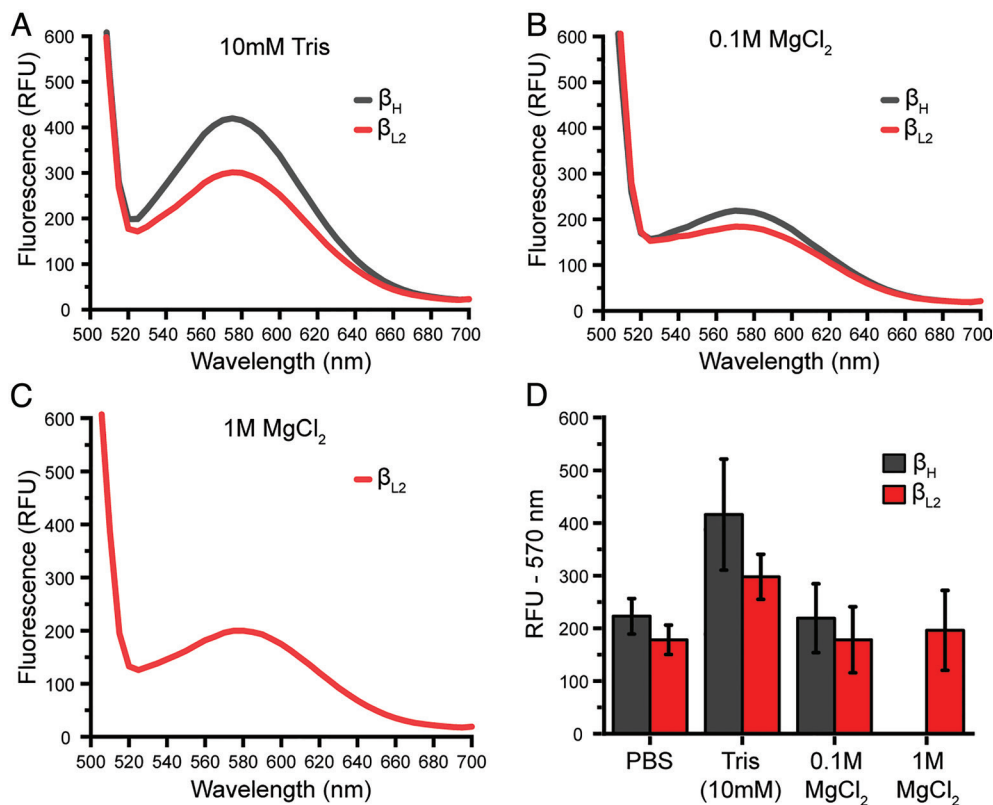


**Fig. 6.** Examination of hydrophobic interfaces in lens  $\beta$ -crystallins through the use of SYPRO Orange fluorescence. Tracking changes in exposed hydrophobic surface area in  $\beta_H$  and  $\beta_{L2}$  through (A) 10 mM Tris, (B) 10 mM Tris + 0.1 M  $\text{MgCl}_2$ , and (C) 10 mM Tris + 1 M  $\text{MgCl}_2$ . Graphs represent the average fluorescent profile of six individual measurements from two biological replicates. Since  $\beta_H$  is completely dissociated in 1 M  $\text{MgCl}_2$ , only fluorescence of  $\beta_{L2}$  was measured at this condition. (D) Comparison of all conditions, including PBS, for both  $\beta_H$  and  $\beta_{L2}$ . Bar graphs represent two batches of three lenses ( $N = 2$ ) and the data are averaged with error bars representing one SD.

favorable, resulting in the dissociation of  $\beta_H$  in favor of  $\beta_{L1}$  and  $\beta_{L2}$ . If true, this could also suggest that through evolution,  $\beta$ -crystallins expressed in the lens exchanged affinity for calcium with the ability to assemble polydisperse, oligomeric structures through conformational changes in the N terminus (75). Additionally, solved structures of lens  $\beta$ -crystallins reveal a solvent-exposed  $\beta$ -strand–binder–random coil motif at the N terminus, which has been shown in other systems to be involved in coordination of divalent cations (78). This motif is also solvent exposed in tetramers (PDB: 2BB2; (50)) and has been shown in other nonlens monomeric crystallins (i.e.,  $\beta\gamma$ -crystallin) to coordinate divalent cations (74). We believe that divalent cations coordinate near protein–protein interfaces, where hydrophobic residues are present and solvent-exposed in  $\beta_H$ . The cation-binding would disrupt these weak protein–protein interfaces, causing dissociation of the larger oligomers. Amino acids expected to be involved in cation-binding may be of interest in future evolutionary studies.

Often crystallins are recruited to the lens through evolution from other proteins and coopted for vision (79–81), and  $\beta$ -crystallins are no exception. In the case of  $\beta\gamma$ -crystallins, there have been recent connections to proteins with calcium-binding function across all domains of life (72, 73, 75, 76, 82–86). This function appears to be evolutionarily conserved in the double Greek-key-folded structure (14, 74, 84, 87). The major effect of cation binding in these other proteins is the increased thermodynamic, kinetic, and mechanical stability (72, 74, 75, 77, 85, 86). The ability of lens  $\beta$ -crystallins to bind calcium has been speculated as a protective and homeostatic function. It has even been proposed that  $\beta$ -crystallins expressed outside of the lens utilize cation binding to respond to cellular stressors (15–17). There is also evidence that these behaviors could extend beyond calcium. In addition to our results with  $\beta$ -crystallins and magnesium, Roskamp et al. showed that  $\gamma$ -crystallin can bind copper ( $\text{Cu}^{2+}$ ) to prevent oxidative damage in the lens (88). While others have confirmed the evolutionarily conserved function of cation-binding in  $\beta\gamma$ -crystallins (74, 75, 87), our data support a relationship between this function and oligomerization.

Because the balance of crystallin subtypes in the vertebrate lens is critical to maintaining transparency (89), it is important to consider the physiological implications of these interactions. Based on homology of  $\beta\gamma$ -crystallins among different organisms, cation binding for lens  $\beta$ -crystallins should involve a mix of sidechain and backbone interactions involving asparagine, serine, threonine, and aspartic and glutamic acid residues (14, 72, 74, 75, 87). Although they may not be directly involved in cation binding, other proximal residues like histidine may also have an important role in mediating protein–protein interactions. Age-related changes such as deamidation (90) may also be specific to these sites, disrupting calcium regulation and resulting in cataract-related changes. It has been well-established that calcium plays a role in cataractogenesis (19, 21, 70, 71, 91, 92), where elevated cation levels result in changes to the morphology, solubility, and permeability of lenticular cell membranes, as well as production of high molecular weight protein aggregates (93–99). Incubation of a lens in  $\text{CaCl}_2$  can also produce aggregates in the lens cortex (71, 100), where  $\beta$ -crystallin concentration is highest. Furthermore, both calcium and magnesium can affect the oligomeric state of  $\alpha$ -crystallin and its chaperone activity (101), suggesting multiple avenues for lens dysfunction when divalent cation-binding is not regulated. When considered with our results, these observations indicate a delicate balance between cation-modulated polydispersity that may be a benefit or detriment to proper lens function. In addition, while we propose cation interactions that may be inherent to  $\beta$ -subtypes and independent of the lens chaperone

$\alpha$ -subtype, these connections should be investigated further. Specifically, what is the function of such uniquely modulated polydispersity in  $\beta$ -crystallins, and what is the need for multiple  $\beta$ -isoforms in the vertebrate lens when other organisms express fewer crystallins but retain optical power (32, 79, 102)? The cation-regulating mechanisms of  $\beta$ -crystallin outlined by our results are expected to contribute to the long-lived stability and transparency of the lens. It is unclear how these changes in quaternary interactions affect local microstructure and how well these features are tolerated with age. Future work will focus on addressing these questions to continue building our understanding of lens development, maturation, and the protein interfaces that enable vision.

## Materials and Methods

**Purification of Lens Crystallins.** Bovine calf eyes (< 2 y) were obtained locally (Research 87 Inc., Boylston, MA) and dissected to harvest each lens. Lenses were either lysed immediately for purification or frozen whole at  $-20^\circ\text{C}$  afterward to be thawed and lysed later within 6 mo. Lens lysis protocol consisted of homogenization in a glass tissue-grinder in PBS, pH 7.3, with 0.2% sodium azide, 5 mM EDTA (Thermo Scientific), and 1 Pierce™ Protease Inhibitor Mini Tablet, EDTA-Free (Thermo Scientific). Lysates were centrifuged at  $25,000 \times g$  and  $4^\circ\text{C}$  for 25 min. Supernatant was loaded onto a Superdex 200 increase 10/300 GL size-exclusion column (Cytiva) attached to an Äkta™ go fast performance liquid chromatography (FPLC) protein purification system (Cytiva). Elution buffer was either PBS or 10 mM Tris (Tris-HCl, Promega) containing  $\text{MgCl}_2$  ( $\text{MgCl}_2$  hexahydrate, Fisher Bioagents), 1 M or 1.5 M NaCl, 1 M  $\text{CaCl}_2$  ( $\text{CaCl}_2$  dihydrate, Fisher Bioagents), or 0.33 M  $\text{Na}_2\text{SO}_4$  (Spectrum). All buffers were adjusted to pH 7.3 using either HCl or NaOH and vacuum-filtered using a 0.22  $\mu\text{m}$  polyvinylidene fluoride (PVDF) membrane. Chromatography was performed at 0.35 mL/min in a refrigerator ( $4^\circ\text{C}$ ), except for purifications with buffer containing 0.33 M  $\text{Na}_2\text{SO}_4$ , which were performed at room temperature and 0.5 mL/min. Fractions were collected by an F9-T fraction collector (Cytiva) in borosilicate glass tubes (Fisherbrand) and kept at  $4^\circ\text{C}$ . All collected samples were used or analyzed within a week after initial thawing.

**SDS-PAGE Analysis.** Samples were prepared with  $2 \times$  Laemmli buffer (Bio-Rad) containing  $\beta$ -mercaptoethanol and boiled at  $95^\circ\text{C}$  for 10 min. Electrophoresis was conducted at 110 V for approximately 80 min. Then, 5 mg total protein was loaded in each lane of a 12% polyacrylamide gel (Bio-Rad). Gel was stained with a solution containing Coomassie Brilliant Blue G250 and destained overnight prior to imaging.

**Cortical and Nuclear Segmenting of Bovine Lens.** Dissection of the nuclear and cortical regions of the lens was performed with a 6-mm biopsy punch (Miltex) and sterile, disposable scalpels. We worked with cold lenses to create a phase separation between the nucleus and cortex to reproducibly remove the nuclear region. The remaining cortex (resembling a donut ring) was then cut and extended lengthwise. These pieces were cut down the middle, resulting in the inner and outer cortical segments. For these experiments, we only used fresh lenses that were never previously frozen. Lysis was performed as described above, and all lysate solutions were equilibrated at approximately 10 mg/mL prior to SEC purification.

**Protein Quantitation Methods.** Protein concentrations were determined using a detergent-compatible (DC) Lowry assay (Bio-Rad) using bovine serum albumin (BSA) dissolved in PBS, pH 7.3 to create a standard curve. Each standard and sample were pipetted in triplicate and averaged. Due to the high concentration of protein in the lens, a 1% dilution in PBS was made each time to estimate the lysate concentrations more accurately. Appropriate dilutions were made for purified crystallin samples.

Area under the curve (AUC) was determined in OriginPro using the Peak Analyzer function. Integration was performed using the minimum absorbance as a baseline. AUC was reported as a percentage of the peak area over total integrated area of the raw data. Normalized chromatograms were not used to determine AUC.

**Mass Spectrometry (LC-MS/MS) and Comparison of  $\beta$ -crystallin Isoform Compositions.** Crystallins purified in PBS, pH 7.3 were diluted with PBS to 0.5 mg in 1 mL total volume. Samples were prepared with  $2 \times$  Laemmli buffer (Bio-Rad)



containing  $\beta$ -mercaptoethanol and boiled at 95°C for 10 min. Five milligrams of total protein were loaded in each lane of a 12% polyacrylamide gel (Bio-Rad). Electrophoresis was conducted at 110 V for approximately 15 min. Gel was stained with a solution containing Coomassie Brilliant Blue G250 and destained overnight. The corresponding lanes were excised, rinsed with milliQ water, and stored in 1.5 mL microcentrifuge tubes with additional milliQ water to prevent dehydration. Samples were shipped to the Shaffer Lab (University of Massachusetts Chan Medical School, Shrewsbury, MA) for further analysis. Excised lanes were trypsinized prior to LC-MS/MS analysis. After overnight digestion and elution of peptides, the samples were lyophilized by speed vacuum and reconstituted in 25  $\mu$ L 5% acetonitrile and 0.2% formic acid in water. Afterward, 3  $\mu$ L of each sample were injected onto the Fusion Lumos Orbitrap MS (both MS and MS/MS) mode. The peptides were searched against the bovine proteome (SwissProt; 20181226, V3) with Mascot Search Engine in Proteome Discoverer 2.1 (Thermo Fisher Scientific) following Scaffold 4 (Proteome Software) for FDR analysis. At 1% false discovery rate (FDR), 319 proteins (227 clusters) were detected across the samples where the first 1–12 proteins were  $\alpha$ ,  $\beta$ , and  $\gamma$ -crystallins.

For  $\beta$ -crystallins, PSM were filtered based on confidence level ( $\geq 95\%$ ) and normalized by dividing the number of PSM by total PSM for that sample. For  $\beta_H$  and  $\beta_{L2}$  purified in PBS, pH 7.3, there were 3,751 and 3,242 total PSM, respectively. These normalized values were used to compare relative isoform abundance between  $\beta_H$  and  $\beta_{L2}$ .

**Isoelectric Point Determination.** Isoelectric points were determined similar to Salgin et al. (69) using a Zetasizer NanoZS90 (Malvern Panalytical Ltd.). Briefly, crystallins purified in PBS were diluted in a custom-made PCCS buffer. This solution suitably buffers across pH 2–8 and has similar ionic strength to PBS at pH 7. For samples prepared in 10 mM Tris containing either 0.01 or 0.1 M  $MgCl_2$ , this buffer was not used to avoid unintended interactions between buffer components and resulted in fewer obtainable data points under these conditions. Final protein concentrations were between 0.1 and 0.7 mg/mL. The zeta-potential of protein

solutions was measured in a disposable folded capillary cell and titrated with 0.1 M HCl or 0.1 M NaOH across pH 3–8. Data were fit with a sigmoidal function in OriginPro to determine the X-intercept where zeta-potential is estimated to be 0 mV, which is the isoelectric point.

**Fluorescent Assay to Quantify Hydrophobic Area.** Lens lysates were injected and eluted in 10 mM Tris containing 0, 0.1 and 1 M  $MgCl_2$ , as well as PBS. Crystallins were collected, pooled based on the subtype, and concentrated via centrifugation using a 10-kDa molecular weight cutoff filter (Millipore Sigma) at 4,000  $\times$  g for 30 min. A DC assay was performed to quantify dilutions of crystallin protein against a BSA standard curve. All crystallins were assayed at 0.5 mg/mL using the appropriate solvent buffer and analyzed in triplicate in a low-UV absorbing 96-well plate (Corning) containing SYPRO Orange (1 $\times$ , Invitrogen) in dimethyl sulfoxide (DMSO). After shaking for 5 s, fluorescence was measured from 500 to 700 nm after excitation at 470 nm. This process was repeated using two batches of three lenses ( $N = 2$ ) and the data are averaged with error bars representing one SD.

**Data, Materials, and Software Availability.** All study data are included in the article and/or *SI Appendix*.

**ACKNOWLEDGMENTS.** This work was supported in part by the National Science Foundation (Award DMR-1712345), the Army Research Office (Award W911NF-16-1-0455), and the Department of Chemistry and Chemical Biology at Northeastern University. Specifically, we acknowledge Prof. Penny Beuning and her research lab for use of their high-speed centrifuge used in our lysis protocol, as well as for conversations regarding chromatography and protein purification methods. We thank Dr. Cassandra Martin and Emily Micheloni for continued discussions about the results and topics of this research. Finally, we would like to acknowledge and thank Kyle Jones, an undergraduate student who assisted with some early experiments that did not produce data for this paper, but the negative results of those experiments seeded the ideas elaborated here.

- P. P. Fagerholm, B. T. Philipson, B. Lindstrom, Normal human lens-the distribution of protein. *Exp. Eye Res.* **33**, 615–620 (1981).
- B. Pierscionek, R. C. Augusteyn, Protein distribution patterns in concentric layers from single bovine lenses: Changes with development and ageing. *Curr. Eye Res.* **7**, 11–23 (1988).
- R. C. Augusteyn, On the growth and internal structure of the human lens. *Exp. Eye Res.* **90**, 643–654 (2010).
- S. Trokel, The physical basis for transparency of the crystalline lens. *Invest. Ophthalmol.* **1**, 493–501 (1962).
- B. K. Pierscionek, D. Y. Chan, Refractive index gradient of human lenses. *Optom. Vis. Sci.* **66**, 822–829 (1989).
- A. K. Kenworthy, A. D. Magid, T. N. Oliver, T. J. McIntosh, Colloid osmotic pressure of steer alpha- and beta-crystallins: Possible functional roles for lens crystallin distribution and structural diversity. *Exp. Eye Res.* **59**, 11–30 (1994).
- F. Veretout, M. Delaye, A. Tardieu, Molecular basis of eye lens transparency. Osmotic pressure and X-ray analysis of alpha-crystallin solutions. *J. Mol. Biol.* **205**, 713–728 (1989).
- F. Veretout, A. Tardieu, The protein concentration gradient within eye lens might originate from constant osmotic pressure coupled to differential interactive properties of crystallins. *Eur. Biophys. J.* **17**, 61–68 (1989).
- A. D. Magid, A. K. Kenworthy, T. J. McIntosh, Colloid osmotic pressure of steer crystallins: Implications for the origin of the refractive index gradient and transparency of the lens. *Exp. Eye Res.* **55**, 615–627 (1992).
- S. A. Hibbert et al., A potential role for endogenous proteins as sacrificial sunscreens and antioxidants in human tissues. *Redox. Biol.* **5**, 101–113 (2015).
- J. Chen, P. R. Callis, J. King, Mechanism of the very efficient quenching of tryptophan fluorescence in human gamma D- and gamma S- crystallins: The gamma-crystallin fold may have evolved to protect tryptophan residues from ultraviolet photodamage. *Biochemistry* **48**, 3708–3716 (2009).
- N. Schafheimer, J. King, Tryptophan cluster protects human gammaD-crystallin from ultraviolet radiation-induced photoaggregation in vitro. *Photochem. Photobiol.* **89**, 1106–1115 (2013).
- J. Vanmarle, R. Jonges, G. F. Vrensen, A. Dewolf, Calcium and its localization in human lens fibres: An electron tomographic study. *Exp. Eye Res.* **65**, 83–88 (1997).
- M. K. Jobby, Y. Sharma, Calcium-binding to lens betaB2- and betaA3-crystallins suggests that all beta-crystallins are calcium-binding proteins. *FEBS J.* **274**, 4135–4147 (2007).
- R. P. Dirks, S. T. Van Genesen, J. J. KrUse, L. Jorissen, N. H. Lubsen, Extralenticular expression of the rodent betaB2-crystallin gene. *Exp. Eye Res.* **66**, 267–269 (1998).
- G. A. Brunekreef, S. T. van Genesen, O. H. Destree, N. H. Lubsen, Extralenticular expression of *Xenopus laevis* alpha-, beta-, and gamma-crystallin genes. *Invest. Ophthalmol. Vis. Sci.* **38**, 2764–2771 (1997).
- A. Coop, K. E. Wiesmann, M. J. Crabbe, Translocation of beta crystallin in neural cells in response to stress. *FEBS Lett.* **431**, 319–321 (1998).
- O. A. Candia, Electrolyte and fluid transport across corneal, conjunctival and lens epithelia. *Exp. Eye Res.* **78**, 527–535 (2004).
- M. Gosak, D. Gotic, E. Spasovska, M. Hawlina, S. Andjelic, Cataract progression associated with modifications in calcium signaling in human lens epithelia as studied by mechanical stimulation. *Life (Basel)* **11**, 369 (2021).
- J. Gao, P. J. Minogue, E. C. Beyer, R. T. Mathias, V. M. Berthoud, Disruption of the lens circulation causes calcium accumulation and precipitates in connexin mutant mice. *Am. J. Physiol. Cell Physiol.* **314**, C492–C503 (2018).
- G. Duncan, T. J. Jacob, Calcium and the physiology of cataract. *Ciba Found. Symp.* **106**, 132–152 (1984).
- G. F. J. M. Vrensen, A. de Wolf, Calcium distribution in the human eye lens. *Ophthalmic. Res.* **28**, 78–85 (1997).
- D. R. Adams, The role of calcium in senile cataract. *Biochem. J.* **23**, 902–912 (1929).
- N. A. Delamere, C. A. Paterson, D. L. Holmes, Hypocalcemic cataract. I. An animal model and cation distribution study. *Metab. Pediatr. Ophthalmol.* **5**, 77–82 (1981).
- M. Gosak et al., The analysis of intracellular and intercellular calcium signaling in human anterior lens capsule epithelial cells with regard to different types and stages of the cataract. *PLoS One* **10**, e0143781 (2015).
- P. D. Gupta, K. Johar, A. Vasavada, Causative and preventive action of calcium in cataractogenesis. *Acta. Pharmacol. Sin.* **25**, 1250–1256 (2004).
- L. L. David, T. R. Shearer, Beta-crystallins insolubilized by calpain II in vitro contain cleavage sites similar to beta-crystallins insolubilized during cataract. *FEBS Lett.* **324**, 265–270 (1993).
- L. L. David, T. R. Shearer, M. Shih, Sequence analysis of lens beta-crystallins suggests involvement of calpain in cataract formation. *J. Biol. Chem.* **268**, 1937–1940 (1993).
- A. A. Swanson, A. W. Truesdale, Elemental analysis in normal and cataractous human lens tissue. *Biochem. Biophys. Res. Commun.* **45**, 1488–1496 (1971).
- M. Delaye, A. Tardieu, Short-range order of crystallin proteins accounts for eye lens transparency. *Nature* **302**, 415–417 (1983).
- A. Tardieu, Eye lens proteins and transparency: From light transmission theory to solution X-ray structural analysis. *Annu. Rev. Biophys. Biophys. Chem.* **17**, 47–70 (1988).
- J. Cai, J. P. Townsend, T. C. Dodson, P. A. Heiney, A. M. Sweeney, Eye patches: Protein assembly of index-gradient squid lenses. *Science* **357**, 564–569 (2017).
- S. H. Chiou, P. Azari, M. E. Himmel, P. G. Squire, Isolation and physical characterization of bovine lens crystallins. *Int. J. Pept. Protein Res.* **13**, 409–417 (1979).
- S. H. Chiou, P. Azari, M. E. Himmel, H. K. Lin, W. P. Chang, Physicochemical characterization of beta-crystallins from bovine lenses: Hydrodynamic and aggregation properties. *J. Protein Chem.* **8**, 19–32 (1989).
- R. J. Siezen, R. D. Anello, J. A. Thomson, Interactions of lens proteins. Concentration dependence of beta-crystallin aggregation. *Exp. Eye Res.* **43**, 293–303 (1986).
- P. G. Cooper, J. A. Carver, R. J. Truscott, 1H-NMR spectroscopy of bovine lens beta-crystallin. The role of the beta B2-crystallin C-terminal extension in aggregation. *Eur. J. Biochem.* **213**, 321–328 (1993).
- C. Slingsby, O. A. Bateman, Rapid separation of bovine beta-crystallin subunits beta B1, beta B2, beta B3, beta A3 and beta A4. *Exp. Eye Res.* **51**, 21–26 (1990).
- J. F. Hejtmancik et al., Association properties of betaB2- and betaA3-crystallin: Ability to form dimers. *Protein Eng.* **10**, 1347–1352 (1997).
- B. F. Liu, J. J. Liang, Protein-protein interactions among human lens acidic and basic beta-crystallins. *FEBS Lett.* **581**, 3936–3942 (2007).
- M. P. Chan, M. Dolinska, Y. V. Sergeev, P. T. Wingfield, J. F. Hejtmancik, Association properties of betaB1- and betaA3-crystallins: Ability to form heterotetramers. *Biochemistry* **47**, 11062–11069 (2008).

41. J. F. Hejtmancik, P. T. Wingfield, Y. V. Sergeev, Beta-crystallin association. *Exp. Eye Res.* **79**, 377–383 (2004).
42. C. Slingsby, O. A. Bateman, Quaternary interactions in eye lens beta-crystallins: Basic and acidic subunits of beta-crystallins favor heterologous association. *Biochemistry* **29**, 6592–6599 (1990).
43. P. G. Cooper, J. A. Aquilina, R. J. Truscott, J. A. Carver, Supramolecular order within the lens: <sup>1</sup>H NMR spectroscopic evidence for specific crystallin-crystallin interactions. *Exp. Eye Res.* **59**, 607–616 (1994).
44. M. S. Ajaz, Z. Ma, D. L. Smith, J. B. Smith, Size of human lens beta-crystallin aggregates are distinguished by N-terminal truncation of betaB1. *J. Biol. Chem.* **272**, 11250–11255 (1997).
45. M. B. Dolinska, Y. V. Sergeev, M. P. Chan, I. Palmer, P. T. Wingfield, N-terminal extension of beta B1-crystallin: Identification of a critical region that modulates protein interaction with beta A3-crystallin. *Biochemistry* **48**, 9684–9695 (2009).
46. J. N. Hope, H. C. Chen, J. F. Hejtmancik, Beta A3/A1-crystallin association: Role of the N-terminal arm. *Protein Eng.* **7**, 445–451 (1994).
47. P. J. Werten, J. A. Carver, R. Jaenicke, W. W. de Jong, The elusive role of the N-terminal extension of beta A3- and beta A1-crystallin. *Protein Eng.* **9**, 1021–1028 (1996).
48. R. C. Kroone *et al.*, The role of the sequence extensions in beta-crystallin assembly. *Protein Eng.* **7**, 1395–1399 (1994).
49. S. Trinkl, R. Glockshuber, R. Jaenicke, Dimerization of beta B2-crystallin: The role of the linker peptide and the N- and C-terminal extensions. *Protein Sci.* **3**, 1392–1400 (1994).
50. B. Bax *et al.*, X-ray analysis of beta B2-crystallin and evolution of oligomeric lens proteins. *Nature* **347**, 776–780 (1990).
51. R. Lapatto *et al.*, High resolution structure of an oligomeric eye lens beta-crystallin. Loops, arches, linkers and interfaces in beta B2 dimer compared to a monomeric gamma-crystallin. *J. Mol. Biol.* **222**, 1067–1083 (1991).
52. V. Nalin *et al.*, Close packing of an oligomeric eye lens beta-crystallin induces loss of symmetry and ordering of sequence extensions. *J. Mol. Biol.* **236**, 1250–1258 (1994).
53. O. A. Bateman, C. Slingsby, Structural studies on beta H-crystallin from bovine eye lens. *Exp. Eye Res.* **55**, 127–133 (1992).
54. T. Takata, J. P. Smith, B. Arbogast, L. L. David, K. J. Lampi, Solvent accessibility of betaB2-crystallin and local structural changes due to deamidation at the dimer interface. *Exp. Eye Res.* **91**, 336–346 (2010).
55. K. J. Lampi, P. A. Wilmarth, M. R. Murray, L. L. David, Lens beta-crystallins: The role of deamidation and related modifications in aging and cataract. *Prog. Biophys. Mol. Biol.* **115**, 21–31 (2014).
56. G. J. Bessems, H. J. Hoenders, The concentration-dependent aggregation of calf and human crystallins. *Exp. Eye Res.* **43**, 1135–1139 (1986).
57. Y. V. Sergeev, J. F. Hejtmancik, P. T. Wingfield, Energetics of domain-domain interactions and entropy driven association of beta-crystallins. *Biochemistry* **43**, 415–424 (2004).
58. M. A. B. Morais *et al.*, Calcium and magnesium ions modulate the oligomeric state and function of mitochondrial 2-Cys peroxidases in Leishmania parasites. *J. Biol. Chem.* **292**, 7023–7039 (2017).
59. F. A. Asselbergs, M. Koopmans, W. J. van Venrooij, H. Bloemendal, Improved resolution of calf lens beta-crystallins. *Exp. Eye Res.* **28**, 223–228 (1979).
60. G. W. Kilby, R. J. Truscott, G. M. Stuchbury, M. M. Sheil, Mass spectrometry of lens crystallins: Bovine beta-crystallins. *Rapid Commun. Mass Spectrom.* **10**, 123–129 (1996).
61. B. Pierscionek, G. Smith, R. C. Augusteyn, The refractive increments of bovine alpha-, beta-, and gamma-crystallins. *Vision Res.* **27**, 1539–1541 (1987).
62. G. J. van Kamp, H. J. Hoenders, The distribution of the soluble proteins in the calf lens. *Exp. Eye Res.* **17**, 417–426 (1973).
63. D. M. Anderson *et al.*, MALDI imaging mass spectrometry of beta- and gamma-crystallins in the ocular lens. *J. Mass Spectrom.* **55**, e4473 (2020).
64. Z. Ma *et al.*, Age-related changes in human lens crystallins identified by HPLC and mass spectrometry. *Exp. Eye Res.* **67**, 21–30 (1998).
65. K. J. Lampi *et al.*, Age-related changes in human lens crystallins identified by two-dimensional electrophoresis and mass spectrometry. *Exp. Eye Res.* **67**, 31–43 (1998).
66. Y. Sharma, D. Balasubramanian, Calcium binding properties of beta-crystallins. *Ophthalmic Res.* **28**, 44–47 (1996).
67. B. Rajini *et al.*, Calcium binding properties of gamma-crystallin: Calcium ion binds at the Greek key beta gamma-crystallin fold. *J. Biol. Chem.* **276**, 38464–38471 (2001).
68. I. A. Tomashevskii, O. A. Golovanova, S. V. Anisina, A spectrophotometric study of the complexation of magnesium(II) with a number of amino acids in aqueous solutions. *Russ J. Gen. Chem.* **91**, 2621–2626 (2021).
69. S. Salgin, U. Salgin, S. Bahadir, Zeta potentials and isoelectric points of biomolecules: The effects of ion types and ionic strengths. *Int. J. Electrochem. Sci.* **7**, 12404–12414 (2012).
70. Y. Sharma *et al.*, Binding site conformation dictates the color of the dye stains-all. A study of the binding of this dye to the eye lens proteins crystallins. *J. Biol. Chem.* **264**, 20923–20927 (1989).
71. J. I. Clark, M. E. Danford-Kaplan, M. Delaye, Calcium decreases transparency of homogenate from lens cortex and has no effect on nucleus. *Exp. Eye Res.* **47**, 447–455 (1988).
72. R. P. Barnwal, M. K. Jobby, K. M. Devi, Y. Sharma, K. V. Chary, Solution structure and calcium-binding properties of M-crystallin, a primordial betagamma-crystallin from archaea. *J. Mol. Biol.* **386**, 675–689 (2009).
73. R. P. Barnwal, G. Agarwal, Y. Sharma, K. V. Chary, Complete backbone assignment of a Ca<sup>2+</sup>-binding protein of the betagamma-crystallin superfamily from Methanosarcina acetivorans, at two denaturant concentrations. *Biomol. NMR Assign.* **3**, 107–110 (2009).
74. K. W. Roskamp, N. Kozlyuk, S. Sengupta, J. C. Bierma, R. W. Martin, Divalent cations and the divergence of betagamma-crystallin function. *Biochemistry* **58**, 4505–4518 (2019).
75. N. Kozlyuk, S. Sengupta, J. C. Bierma, R. W. Martin, Calcium binding dramatically stabilizes an ancestral crystallin fold in tunicate betagamma-crystallin. *Biochemistry* **55**, 6961–6968 (2016).
76. M. Kretschmar, E. M. Mayr, R. Jaenicke, Homo-dimeric spherulin 3a: A single-domain member of the beta gamma-crystallin superfamily. *Biol. Chem.* **380**, 89–94 (1999).
77. Z. N. Scholl, Q. Li, W. Yang, P. E. Marszalek, Single-molecule force spectroscopy reveals the calcium dependence of the alternative conformations in the native state of a betagamma-crystallin protein. *J. Biol. Chem.* **291**, 18263–18275 (2016).
78. V. V. Khrustalev, E. V. Barkovsky, T. A. Khrustaleva, Magnesium and manganese binding sites on proteins have the same, predominant motif of secondary structure. *J. Theor. Biol.* **395**, 174–185 (2016).
79. G. Wistow, C. Slingsby, Structure and evolution of crystallins. *Encycl. Eye* **32**, 229–238 (2010).
80. G. J. Wistow, J. Piatigorsky, Lens crystallins: The evolution and expression of proteins for a highly specialized tissue. *Annu. Rev. Biochem.* **57**, 479–504 (1988).
81. J. Piatigorsky, Gene sharing, lens crystallins and speculations on an eye/ear evolutionary relationship. *Integr. Comp. Biol.* **43**, 492–499 (2003).
82. M. K. Jobby, Y. Sharma, Calcium-binding crystallins from Yersinia pestis. Characterization of two single betagamma-crystallin domains of a putative exported protein. *J. Biol. Chem.* **280**, 1209–1216 (2005).
83. M. E. Ray, G. Wistow, Y. A. Su, P. S. Meltzer, J. M. Trent, AIM1, a novel non-lens member of the betagamma-crystallin superfamily, is associated with the control of tumorigenicity in human malignant melanoma. *Proc. Natl. Acad. Sci. U.S.A.* **94**, 3229–3234 (1997).
84. B. Rajini, C. Graham, G. Wistow, Y. Sharma, Stability, homodimerization, and calcium-binding properties of a single, variant betagamma-crystallin domain of the protein absent in melanoma 1 (AIM1). *Biochemistry* **42**, 4552–4559 (2003).
85. M. Wenk, E. M. Mayr, Myxococcus xanthus spore coat protein S, a stress-induced member of the betagamma-crystallin superfamily, gains stability from binding of calcium ions. *Eur. J. Biochem.* **255**, 604–610 (1998).
86. M. Kretschmar, E. M. Mayr, R. Jaenicke, Kinetic and thermodynamic stabilization of the betagamma-crystallin homolog spherulin 3a from Physarum polycephalum by calcium binding. *J. Mol. Biol.* **289**, 701–705 (1999).
87. P. Aravind *et al.*, The betagamma-crystallin superfamily contains a universal motif for binding calcium. *Biochemistry* **48**, 12180–12190 (2009).
88. K. W. Roskamp *et al.*, Human gammaS-crystallin-copper binding helps buffer against aggregation caused by oxidative damage. *Biochemistry* **59**, 2371–2385 (2020).
89. P. W. N. Schmid *et al.*, Imbalances in the eye lens proteome are linked to cataract formation. *Nat. Struct. Mol. Biol.* **28**, 143–151 (2021).
90. K. Zhang, X. Zhu, Y. Lu, The proteome of cataract markers: Focus on crystallins. *Adv. Clin. Chem.* **86**, 179–210 (2018).
91. V. Haykin *et al.*, Bioimage analysis of cell physiology of primary lens epithelial cells from diabetic and non-diabetic cataract patients. *Biotechnol. Biotech. Eq.* **35**, 170–178 (2021).
92. Y. X. Li, D. Y. Parkinson, J. Feng, C. H. Xia, X. H. Gong, Quantitative X-ray tomographic analysis reveals calcium precipitation in cataractogenesis. *Sci. Rep.* **11**, 17401 (2021).
93. F. J. Giblin, K. R. Hightower, P. A. Ragatzki, V. N. Reddy, Calcium-induced high molecular-weight proteins in the intact rabbit lens. *Exp. Eye Res.* **39**, 9–17 (1984).
94. J. A. Jedziniak, J. H. Kinoshita, E. M. Yates, L. O. Hocker, G. B. Benedek, Calcium-induced aggregation of bovine lens alpha crystallins. *Invest. Ophthalmol.* **11**, 905–915 (1972).
95. A. Spector, D. Adams, K. Krul, Calcium and high molecular weight protein aggregates in bovine and human lens. *Invest. Ophthalmol.* **13**, 982–990 (1974).
96. J. Alcalá, J. Valentine, H. Maisel, Human lens fiber cell plasma membranes. I. Isolation, polypeptide composition and changes associated with ageing. *Exp. Eye Res.* **30**, 659–677 (1980).
97. H. Bloemendal, A. J. Vermorken, M. Kibbelaar, I. Dunia, E. L. Benedetti, Nomenclature for the polypeptide chains of lens plasma membranes. *Exp. Eye Res.* **24**, 413–415 (1977).
98. R. M. Broekhuyse, E. D. Kuhlmann, J. Bijvelt, A. J. Verkleij, P. H. Ververgaert, Lens membranes III. Freeze fracture morphology and composition of bovine lens fibre membranes in relation to ageing. *Exp. Eye Res.* **26**, 147–156 (1978).
99. A. Lasser, E. A. Balazs, Biochemical and fine structure studies on the water-insoluble components of the calf lens. *Exp. Eye Res.* **13**, 292–308 (1972).
100. J. I. Clark, L. Mengel, A. Bagg, G. B. Benedek, Cortical opacity, calcium concentration and fiber membrane structure in the calf lens. *Exp. Eye Res.* **31**, 399–410 (1980).
101. N. A. Chebotareva, T. B. Eronina, N. N. Sluchanko, B. I. Kurganov, Effect of Ca<sup>2+</sup> and Mg<sup>2+</sup> ions on oligomeric state and chaperone-like activity of alphaB-crystallin in crowded media. *Int. J. Biol. Macromol.* **76**, 86–93 (2015).
102. W. H. Tan *et al.*, Structure of a highly active cephalopod S-crystallin mutant: New molecular evidence for evolution from an active enzyme into lens-refractive protein. *Sci. Rep.* **6**, 31176 (2016).